Nanoporous CeO 2 –ZrO 2 Oxides for Oxidation of Volatile Organic Compounds

Florian Jonas, Bénédicte Lebeau, Stéphane Siffert, Laure Michelin, Christophe Poupin, Renaud Cousin, Ludovic Josien, Loïc Vidal, Martine Mallet, Pierrick Gaudin, et al.

Nanoporous CeO_2-ZrO_2 Oxides for Volatile Organic Compounds Oxidation

Florian Jonas[1], Bénédicte Lebeau[2,3*], Stéphane Siffert[4*], Laure Michelin[2,3], Christophe Poupin[4], Renaud Cousin[4], Ludovic Josien[2,3], Loïc Vidal[2,3], Martine Mallet[5], Pierrick Gaudin[1], Jean-Luc Blin[1*]

[1]: Université de Lorraine, CNRS, L2CM, F-54000 Nancy, France
[2]: Université de Haute Alsace (UHA), CNRS, IS2M UMR 7361, F-68100 Mulhouse, France
[3]: Université de Strasbourg, 67000 Strasbourg, France
[4]: Université du Littoral Côte d'Opale, U.R. 4492, UCEIV, SFR Condorcet FR CNRS 3417, F-59140 Dunkerque, France
[5]: Université de Lorraine, CNRS, LCPME, F-54000 Nancy, France

* Corresponding authors :
Pr. Jean-Luc Blin
Université de Lorraine
L2CM 7053
Faculté des Sciences et Technologies
BP 70239
F-54506 Vandoeuvre-lès-Nancy cedex, France
Tel. +33 3 83 68 43 70
E-mail: Jean-Luc.Blin@univ-lorraine.fr

Dr. Bénédicte Lebeau
Université de Haute Alsace (UHA), CNRS, Axe Matériaux à Porosité Contrôlée (MPC), Institut de Science des Matériaux de Mulhouse (IS2M), UMR 7361, ENSCMu
3bis rue Alfred Werner
F-68093 Mulhouse cedex, France
Tel. +33 3 89 33 68 82
E-mail: Benedicte.Lebeau@uha.fr

Pr. Stéphane Siffert
Unité de Chimie Environnementale et Interactions sur le Vivant (UCEIV) UR-4492
Equipe "Traitement catalytique et énergie propre"
MREI 1 - Université du Littoral - Côte d'Opale
145, avenue Maurice Schumann
59140 Dunkerque
Tel. + 33 3 28 65 82 56
E-mail: stephane.siffert@univ-littoral.fr

Abstract

Here, mixed nanostructured ceria/zirconia oxides have been prepared either by wet impregnation on a nanostructured ZrO_2 or by co-condensation through an EISA-derived pathway. This latter method and the impregnation on amorphous ZrO_2 followed or not by a heating at 480°C lead to a uniform cerium distribution in the zirconia framework and solid solutions are formed. Stabilization of the tetragonal structure of nano ZrO_2 with the increase of the cerium content is observed by XRD and Raman spectroscopy. The surface Ce/Zr molar ratio determined by XPS is very closed to the bulk one, calculated from the X-ray fluorescence analysis. On the opposite, the appearance of nano sized ceria particles with the increase of the cerium content, a monoclinic/tetragonal mixture and an enrichment of the surface in cerium are noted if the impregnation is carried out on a nanostructured ZrO_2 previously calcined at 480°C.

The obtained catalysts have been tested for the oxidation of toluene, used as a model volatile organic compound. The catalytic efficiency of the mixed oxides has also been compared to the one of a pure commercial ceria. Results show that the preparation method has a significant effect on the catalytic properties of the materials. Although pure ceria presents the best activity and selectivity, the nanostructured ZrO_2 previously calcined at 480°C and impregnated by 10 mol% of CeO_2 is almost as efficient as pure ceria.

Keywords : nanostructured materials; Soft templating; Solid solution; Catalyst; Toluene oxidation

1. Introduction

Ceria and zirconia are well known and widely investigated for their great interest for industrial applications[1-9]. For example, ZrO_2 is extensively used in the field of solid oxide fuel cell, microelectronic, luminescent nanoprobe and catalyst[1-6]. As for CeO_2, it is a major component of the three way catalysts used in automotive exhaust gas treatment[7-9]. Due to their redox properties ceria-based materials have also a large capacity for oxygen storage or/and release, which make them excellent candidates as catalysts for volatile organic compounds (VOCs) oxidation[9,10]. VOCs are a major environmental concern, because of their carcinogenic and toxic effects on human health. However, ceria is known to have a poor thermal stability. Introduction of zirconium into the ceria lattice enhances its thermal stability and has a beneficial effect on its redox properties[10]. Mixed CeO_2-ZrO_2 oxides have thus been considered in literature in particular for oxidation reactions[10,12-16], which are favored by the presence of defect induced by the substitution of Ce^{4+} by Zr^{4+}. For example, Gaálová and coll [12] have reported the total oxidation of toluene using platinum deposited on $Ce_{0.5}Zr_{0.5}O_2$ support. The introduction of cerium into zirconia can stabilize its tetragonal and cubic phases at room temperature[17].

Different strategies such as the solid state reaction, the milling, the citrate, the wet impregnation, the sol gel or the precipitation methods have been developed to get these mixed oxides[10,17-20]. Among them chemical ones usually lead to the formation of more homogeneous materials. Catalytic efficiency will be affected by different parameters such as the Ce/Zr ratio, the morphology, the size, the homogeneity of the catalyst or the crystallographic nature of the phase formed, which will depend on the preparation procedure[10,17,21,22]. For example, Wongkasemjit and coll[22] have shown that the activity for CO oxidation of $Ce_xZr_{1-x}O_2$ catalysts decreases with the increase of the Ce/Zr ratio. In addition to thermal stability, the specific surface area, is another important parameter that should be considered for application

of these materials in catalysis, in particular when they are used as supports, for example, for the deposition of platinum or gold[15,23,24]. To increase specific surface area for a better accessibility to active site and to improve mass transport, the introduction of controlled mesoporosity is an efficient way[25]. From this point of view, nanostructured oxides are excellent candidates since they have high specific surface area, large pore volume and tunable pores sizes. These materials can be prepared according to either hard or soft templating methods[26]. For example, Jiaheng and coll [27] have reported the preparation of $Ce_{0.8}Zr_{0.2}O_2$ by the replica of the KIT-6 silica material, which acts as a mold for the ceria-zirconia mixed oxide. Comparing with the equivalent non porous material, the templated $Ce_{0.8}Zr_{0.2}O_2$ exhibits a higher activity for the soot oxidation. The authors have attributed this fact to a better diffusion of oxygen thanks to the presence of the mesopores[27]. Among the soft pathways, the evaporation induced self-assembly (EISA) method is one of the most synthetic routes in the research area of surfactant-assisted mesoporous materials[28]. Initially, it has been developed for mesostructured silica films before being expanded to the non-silica oxides, in particular to CeO_2-ZrO_2 ones[29]. Further, this synthesis pathway was also applied to preparation of powdered materials. In that case amphiphilic block copolymers are mainly used as templates[30]. Lu and coll [31] combined the EISA and the co-precipitation methods to form $Ce_{1-x}Zr_xO_2$ solid solutions with high thermal stability (≈ 1000°C) and homogeneous disordered mesopores, which have a pore diameter around 4 nm. The surfactants Pluronic P123 $((EO)_{20}$-$PO)_{70}$-$(EO)_{20}$ with EO = ethylene oxide and PO = propylene oxide), $C_{16}(EO)_{10}$ (C_{16} = $C_{16}H_{33}$) or CTABr (cetyltrimethylammonium bromide) have been used as templates in the presence of zirconium n-propoxide and ammonium cerium nitrate as zirconia and cerium sources, respectively. The authors have noted no major effect of the template on the mesopore size and arrangement or on the thermal stability. More recently, through EISA route, Deng and coll [24] obtained large interconnected mesopores (> 10 nm) and high specific surface area ceria-

zirconia solid solutions templated by amphiphilic poly(ethylene oxide)-b-polystyrene block copolymer. The prepared mixed nanoporous oxides serve as supports for the dispersion of platinum particles (4 nm of diameter). The authors have reported that the formulated catalysts exhibit an excellent stability (over 50 cycles) and a T_{100} value of 130 °C for the CO oxidation.

The increase of the demand of ceria-based materials in technology and the fact that the cerium production is focused only on a few countries, mainly in China, have involved these last years an increase of the price of ceria materials[32]. The optimization of the cerium content is thus worth of investigation, in particular from the economical point of view, to design highly efficient ceria-based catalyst containing an amount of cerium as low as possible. One strategy to reach this goal consist in dispersing ceria on a support[32-34]. For example, Calvino et al. have deposited ceria on commercial zirconia or yttria-doped zirconia nanocrystals[34]. Both supports have low specific surface area 78 and 89 m²/g, respectively. As explained above, the specific surface area is an important parameter that affect the catalytic activity. Thus, the synthesis of a catalyst by dispersing CeO_2 active phase on the large and accessible surface of thermally stable supports such as nanostructured ZrO_2 appears as a promising strategy to get efficient catalysts for VOC oxidation containing low amount of ceria. Recently, through an EISA-derived procedure, we have reported the preparation of nanostructured ZrO_2 with high thermal and hydrothermal stability[35]. Zirconia materials are obtained by a soft-templating method using Pluronic P123 and zirconium n-propoxide as templating agent and zirconia source, respectively. In order to meet the objective of decreasing the ceria content while preserving the catalytic activity, here, these nanostructured zirconia materials have been used to design nanoporous CeO_2-ZrO_2 catalysts, which have been tested for the toluene oxidation, used as a model volatile organic compound (VOC). As explained above the properties of the mixed oxides and their catalytic efficiency will depend on the preparation method, so to investigate

this parameter the nanoporous CeO_2-ZrO_2 materials have been prepared either by co-condensation or by impregnation.

2. Materials and methods

The triblock copolymer Pluronic P123 $(EO)_{20}(PO)_{70}(EO)_{20}$ (EO = ethylene oxide, PO = propylene oxide), the cerium acetate $Ce(CH_3CO_2)_3$ H_2O and the zirconium isopropoxide (70 wt.% in propanol) were purchased from Aldrich.

2.1. Materials preparation:

Co-condensation route (CC): 2 g of Pluronic P123 are dissolved in 20 mL of ethanol. Then, 2 g of a nitric acid solution (HNO_3, 15M), 4.65 g of zirconium propoxide (Sigma-Aldrich, 70 wt% in propan-1-ol) and y g of cerium acetate are introduced into the solution (y was defined to adjust the cerium content from to 0 to 10 mol.% compared to Zr content). The other steps of the preparation, in particular the P123 extraction in ethanol, are similar to those described for the pure mesostructured ZrO_2 reported in reference 35. The obtained materials have been calcined in a tubular furnace at 480°C under synthetic air at a flow rate of 0.5 L / min. First, the temperature is increased up to 150°C at a rate of 1°C/ min. Then a 1-hour plateau at this temperature is made before reaching 480°C at a rate of 1°C/ min. The sample is then left at 480 ° C for 1 hour. 480°C corresponds to the temperature at which the walls of amorphous zirconia begin to crystallize[35].

Impregnation route: Before impregnation, the bare mesostructured ZrO_2 has been prepared according the same procedure than the one described above for the co-condensation route. Under these conditions, the obtained zirconia is amorphous. The impregnation has been carried out on the amorphous mesostructured ZrO_2, followed (AI-480) or not (AI) by a heating at 480°C. x g of cerium acetate are dissolved in 3 mL of distilled water (x was defined

to adjust the cerium content from to 0 to 10 mol.% compared to Zr content). The solution is then deposited on 1 g of mesostructured zirconia. The obtained paste is mixed and then placed at 80 °C for 12 h. After drying, the materials are calcined, using a similar program than the one applied for the co-condensation method, at 300°C to decompose the cerium precursor. We have shown that at this temperature the mesostructured zirconia remains amorphous[33]. Impregnation has been also realized on a mesostructured ZrO_2 previously calcined at 480°C (CI).

The following notations will be used in the whole text for the different synthesis methods: CC = co-condensation, CI = impregnation on mesostructured ZrO_2 calcined at 480°C, AI = impregnation on amorphous mesostructured ZrO_2 and AI-480 = impregnation on amorphous mesostructured ZrO_2 followed by a heating at 480°C. The different preparation routes are illustrated in Scheme 1.

2.2. Characterization:

The synthesized oxides have been characterized by XRD, SAXS, nitrogen adsorption/desorption analysis using the same equipment (SAXSess mc² instrument from Anton Paar, X'Pert PRO diffractometer equipped with a Cu X-ray tube ($\lambda_{Cu(K\alpha)}$ = 0.1542 nm) operating at 45 kV and 40 mA and a X'Celerator detector from PANalytical and TRISTAR 3000 sorptometer from Micromeritics, respectively) and conditions than the ones reported in reference 35. After degassing at room temperature for 18 h, the nitrogen adsorption/desorption isotherms were recorded at -196°C. The specific surface area was determined by using the BET model in the 0.05-0.20 p/p° region, whereas the pore diameter and the pore size distribution were determined by the BJH (Barret, Joyner, Halenda) method with KJS (Kruk, Jaroniec, Sayari) correction applied to the adsorption branch.

X-ray photoelectron spectrometry (XPS) was used to characterize the physicochemical properties of the synthesized oxides. Spectra were collected on a Kratos Axis Ultra (Kratos Analytical, U.K.) spectrometer equipped with a monochromatic Al Kα source (1486.6 eV) operated at power level of 120W. The analysis area was equal to 300 x 700 μm^2. High–resolution Ce 3d, Zr 3d and O 1s spectra were recorded at a pass energy of 20 eV. A short acquisition time was used to examine Ce 3d region in order to limit photoreduction of Ce^{4+} species during the analyses. Binding energies were calibrated by assigning the adventitious carbon C1s peak to 284.6 eV. Curve fitting was performed using a Gaussian/Lorentzian (70/30) peak shape after Shirley's background subtraction and using X-vison 2.2.11 software.

Raman spectra were collected at 1064 nm on a FRA-106 S FT-Raman (Bruker) coupled on a Equinox IFS 55 FTIR spectrophotometer. The laser power on the sample was 140 mW for 300 scans. The spectral resolution was 4 cm^{-1}.

The Ce/Zr molar ratios were determined using X-ray fluorescence spectrometry (XRF) performed on a PANalytical equipment model Zetium.

Transmission Electron Microscopy (TEM) images and EDX (Energy Dispersive X-ray) chemical analyses were performed using a JEOL ARM200-CFEG microscope operating at 200 kV. The EDX analyses and element mappings were performed using a JEOL Centurio detector.

Ce and Zr element mappings were also recorded by Scanning Electron Microscopy (Philips FEG XL30) coupled with Energy Dispersive X-ray Spectroscopy (EDS).

2.3. Catalytic tests:

Toluene oxidation was carried out in a continuous-flow fixed-bed reactor with 100 mg of catalyst at atmospheric pressure. This amount is sufficient to have a suitable bed height and reproducible results considering possible heterogeneity of the prepared samples. This has

been validated by several tests which were repeated and showed identical results. The gas mixture composed of 1000 ppm of toluene in air (volume ppm) pass through a reactor with a flow rate of 100 mL.min^{-1}, which corresponds to a gas hourly space velocity (GHSV) of about 30.000 h^{-1}. Before each test, the catalysts were pre-activated at 300 °C for 1 hour under flowing air (33 mL.min^{-1}). After reaching a stable flow, reactants were passed through the catalyst bed and the temperature was increased from room temperature to 400 °C at 1 °C min^{-1}. The feed and the reactor outflow gases were analysed with a micro-GC (Agilent 490MicroGC) coupled to an infrared analyser (ADEV CO_2-CO Analyser Model 4400IR) for CO_2 and CO selectivities. For a better comparison of the catalyst the specific activity (Γ_a) and intrinsic activity ($\Gamma_{intrinsic}$) at T_{10} were calculated by:

$$\text{Specific activity : } \Gamma_a = \frac{Q}{Vm} \text{ x } \frac{273.15}{T_{10}} \text{ x } \frac{[\text{Toluene}]_0}{10^6} \text{ x } \frac{\tau_{conversion}}{m_{catalyst}}$$

$$\text{Intrinsic activity : } \Gamma_{intrinsic} = \frac{\Gamma_a}{S_{BET}}$$

Where Q = Volume flow (L/min)

V_m = molar volume (22.4 L/mol)

$[Toluene]_0$ = initial concentration of toluene (1000 ppm)

$\tau_{conversion}$ = Conversion rate of toluene at T_{10}

$m_{catalyst}$ = weight of the catalyst (g)

S_{BET} = Specific surface area (m²/g)

T_{10} is the temperature at which the conversion rate of toluene is equal to 10%.

3. Results and discussion

3.1. Structural and textural characterization of the ZrO_2-CeO_2 materials

From the X-ray diffractograms, depicted in Figure 1, it appears that materials prepared by co-condensation (CC) (Fig. 1A) or by impregnation on the amorphous ZrO_2 followed by a

heating at 480°C (AI480) (Fig. 1D) behave in a similar way. Up to 1 mol.% of cerium, a mixture of tetragonal and monoclinic phases is obtained. Increasing the cerium content, the (110), (-111), (-112), (-202) and (-301) reflections of the monoclinic ZrO_2[36,37] disappear (m-ZrO_2, ICDD card no. 00-037-1484) and only the diffraction lines located at 2θ = 30.1, 34.9, 50.2, 59.7 and 62.8° are observed. They can be respectively attributed to the (101), (002)(110), (112), (103)(211) and (202) reflections of the tetragonal structure (t-ZrO_2, ICDD card no. 04-005-4207)[36]. Therefore, the increase of the cerium content beyond 1 mol.% stabilizes the tetragonal structure. The observation of a single crystallographic phase suggests that zirconium and cerium are homogeneously distributed in the material. The stabilization of the tetragonal structure with the increase of the cerium content is in good accordance with literature and supports the substitution of Zr^{4+} by Ce^{4+} and/or Ce^{3+}. Indeed, it is well known that the dilatation of the cation network induced by the substitution of Zr^{4+}, which has an ionic radius of 0.84 Å for a coordination number equal to 8[38], by a cation having a higher ionic radius such as Ce^{4+} (0.97 Å) or Ce^{3+} (1.14 Å)[38] favors the formation of the tetragonal structure[39-41]. Oxygen vacancies[41,42] that could be created by the reduction of Ce^{4+} and the crystallite size[43,44] can also participate to the stabilization process. Moreover, when the cerium content is raised, a shift towards lower 2θ values of the (101) tetragonal diffraction line is noted for samples prepared from the CC route (Fig. S1A) and for the mixed oxide containing 10 mol.% of cerium synthesized from the AI480 route (Fig. S1C), strengthening the hypothesis of a $Ce_xZr_{1-x}O_2$ solid solution formation for theses nanoporous CeO_2-ZrO_2 materials. In addition, for the material prepared by impregnation on the amorphous ZrO_2 followed by a heating at 480°C (AI480), the tetragonal solid solution $Ce_{0.1}Zr_{0.9}O_2$ has been clearly identified by XRD (t-ZrO_2, ICDD card no. 04-006-7959). For the others methods and cerium loading no solid solution is obtained. This is the reason why the significant shift of the position of the (101) tetragonal diffraction line is noted in Fig. S1A and in Fig. S1C for the

10% sample. For 1 mol.% of cerium, there is thus the coexistence of the tetragonal $Ce_xZr_{1-x}O_2$ solid solution with the monoclinic ZrO_2.

These results are further confirmed by Raman analysis (Fig. S2). Indeed, on the Raman spectra of the bare ZrO_2 or of the samples prepared in the presence of 1 mol.% of cerium (Fig. S2A and S2D), the vibrations observed at 177, 188, 222, 306, 331, 345, 381, 477, 505, 537, 614 and 632 cm^{-1} are assigned to the 9 A_g and 9 B_g modes of the monoclinic ZrO_2[36,45], while the band at 150 cm^{-1} is due to B_{1g} mode of the tetragonal symmetry of the solid solution[45]. Above 1 mol.% of Ce, the peaks detected at 149, 267, 319, 465 and 635 cm^{-1} are associated with the A_{1g}, $2B_{1g}$ and $3E_g$ modes of the tetragonal phase[36,45]. The weak peaks observed in the range 170-200 cm^{-1} are likely due to trace of monoclinic zirconia, which is not detected by XRD.

By contrast, no crystalline phase is detected neither by XRD (Fig. 1C) nor by Raman spectroscopy (Fig. S2C) when the impregnation is carried out on the amorphous ZrO_2 (AI). This result is in accordance with our previous study dealing with the synthesis of mesostructured zirconia with high (hydro)thermal stability. Indeed, in that case materials have been calcined only at 300°C to decompose the cerium precursor and we have shown that at this temperature the mesostructured zirconia is still amorphous. No crystalline ceria particles are observed, suggesting a homogeneous dispersion of the cerium species on the surface of the amorphous mesostructured ZrO_2.

If the impregnation is performed on the calcined zirconia (CI), both XRD (Fig. 1B) and Raman (Fig. S2B) show the coexistence of the monoclinic and tetragonal structures. In addition, no shift of the (101) reflection is observed (Fig. 2B) indicating that in that case no solid solution is formed. Moreover, the diffraction lines detected at 2θ = 28.6, 32.9, 47.6, 56.5° from 10 mol.% of cerium, can be attributed respectively to (111), (200), (220) and (311)

reflections of the cubic CeO_2 (ICDD card no. 00-043-1002) [22]. These diffraction lines ~~peaks~~ become more intense with the increase of cerium content.

The formation of the cerium oxide is also revealed by the very intense vibration observed at 462 cm^{-1} on the Raman spectrum[21] (Fig. S2B), which is assigned to F_{2g} mode of the cubic ceria.

Whatever the material, only one broad line is observed on the SAXS patterns depicted in Figure S3. As reported by Pinnavaia and coll [46], the presence of this single reflection indicates that the CeO_2-ZrO_2 oxides adopt a wormhole mesostructure as observed for the bare zirconia[35]. For a set of samples, no significant change in the d-spacing value is noted with the loading of Ce. For example, considering the solid solution prepared by the co-condensation method the Bragg's distance varies from 5.8 to 5.6 nm when the targeted cerium content is changed from 1 to 10 mol.% (Fig. S3A). As it could be expected, since only a calcination at 300°C has been performed to decompose the cerium precursor, the materials synthesized from the amorphous zirconia present a line at a higher d values (Fig. S3C), therefore in this case the shrinkage of the mesopore network is less pronounced. The disordered mesopore arrangement is confirmed by the TEM analysis. In Figure S4 are given as example the TEM images of samples prepared in the presence of 10 mol.% of cerium.

A type IV isotherm with a H2 hysteresis loop, which is usually observed for wormhole-like structure according to the IUPAC classification[47], is obtained by nitrogen adsorption/desorption without observation of any phenomenon due to pore blocking such as catastrophic desorption (Fig. S5). In a general way, a decrease of the pore volume determined at $p/p° = 0.99$ is noted upon addition of cerium. Taking into account the error on the measurement, about 5%, we can see from Figure S6 and Table S1 that there is no significant change of the mesopore diameter as a function of the cerium loading and that mixed oxides have a similar pore size than the bare zirconia. This indicates that there is no pore blocking

due to the presence of CeO_2 particles. Although they have mesopore diameters in the same range of order (Fig. S6 and Table S1) and compared to the mixed oxides obtained by co-condensation or from impregnation on the calcined ZrO_2, the broad reflection observed on the SAXS pattern of the materials impregnated on the amorphous ZrO_2 and followed by a heating at 480°C is located at lower q value (Fig. S3D), i.e. higher correlation distance. Since the position of this reflection represents the sum of the mesopore diameter and the wall thickness it can be inferred that these materials have a larger wall thickness. For example, for a targeted 5 mol.% of Ce its value is 3.1 nm, against around 2.6 nm for the ones of mesostructures obtained by co-condensation or impregnation on the calcined ZrO_2. CeO_2-ZrO_2 samples have a specific surface area in the range 160-180 m²/g and a pore volume between 0.14 and 0.18 cm^3/g-STP (Table S1).

Mixed-oxides obtained after impregnation on the amorphous mesostructured zirconia have the highest specific surface area and pore volume, in the range of 230-270 m²/g and 0.20-0.30 cm^3/g-STP, respectively (Table 1). After heating at 480°C, the values of these parameters decrease to 160-176 m²/g and to 0.14-0.18 cm^3/g-STP (Table S1) because of crystallization of the walls.

It should also be noted that the t-plot method has been applied on all isotherms and no microporosity was observed. Therefore, the mesopore surface can be assimilated to the BET surface area.

3.2. Quantification of the cerium amount and dispersion of the cerium phase

Whatever the preparation method and the cerium content, Ce 3d high resolution XPS spectra of all materials exhibit the same complex features due to multiple states arising from different Ce 4f level occupancies in the final state and the presence of both Ce(III) and Ce(IV) surface species[48]. Figure 2 depicts the typical ones obtained for a 5 mol.% of cerium in the starting

mixture. All spectra are fitted with five spin-orbit doublets in agreement with the presence of Ce^{4+} (3 pairs of spin-orbit doublets) and Ce^{3+} (2 pairs of spin-orbit doublets). The labels reported in figure 2 follow the commonly used convention established by Burroughs et al[49], in which v and u refer to the $3d_{5/2}$ and $3d_{3/2}$ spin orbital components respectively. The presence of Ce^{4+} is attributed to the three main $3d_{5/2}$ features at 882.6 (ν) 889.7 (ν'') and 898.1 (v''') and the three main features $3d_{3/2}$ at 900.9 (u), 908.1 (u'') and 916.5 eV (u''') [13,21]. The intensity ratio I $3d_{5/2}$/I $3d_{3/2}$ is fixed to 1.5. By contrast, the two main $3d_{5/2}$ features at 880.6 (ν_0) and 885.1 (ν') and the two main $3d_{3/2}$ features at 899.1 (uo) and 903.5 eV (u')- characterize the presence of Ce(III) [13,21].

An important point concerning the mixed ceria/zirconia oxides powders is the photoreduction process taking place under X-rays during analyses[50] despite great care was taken in the present study to limit this process (short acquisition time and limited X-Ray power). Because of the partial photoreduction of Ce^{4+} the ratio of Ce^{4+}/Ce^{3+} cannot be precisely determined and the values reported in Table 1 are given as an indication. In a general way, we can observe that the proportion of Ce^{4+} increases with the cerium content. When the mixed oxides are obtained by wet impregnation on the amorphous ZrO_2, we have shown by XRD that a further heating at 480°C leads to the formation of the solid solution. It can be deduced from Table 1 that the diffusion of cerium into the zirconia is accompanied by a reduction of Ce^{4+} since the Ce^{4+}/Ce^{3+} ratio decreases after the heating process. For example, considering the 0.05 targeted Ce/Zr ratio after wet impregnation on amorphous zirconia the Ce/Zr ratio is equal to 1.1 and it drops to 0.7 after the further heating at 480°C.

Typical Zr 3d and O 1s spectra are represented as example in Figure S7. Two contributions are noted on the Zr 3d spectrum (Fig. S7). The first one, characterized by a doublet at around 181,9 (Zr $3d_{5/2}$) and 184.4 eV (Zr $3d_{3/2}$) is due to ZrO_2 and/or CeO_2-ZrO_2 mixed oxides. The second doublet located at 182.9 and (Zr $3d_{5/2}$) and 185.3 eV (Zr $3d_{3/2}$) arises from zirconium

hydroxide (Zr-OH)[51]. The O 1s spectra can be decomposed into 3 components (Fig. S7) with maxima located at 529.7, 531.5 and 532.8 eV. Referring to literature, they can be attributed to lattice oxygen (O^{2-}), surface oxygen such as hydroxyl group or defect oxide and adsorbed water, respectively[52].

XPS measurements also allow to determine the surface Ce/Zr molar ratio, which can be compared with the bulk composition obtained by X-ray fluorescence (XRF) (Table 1). Whatever the preparation method, the targeted Ce/Zr molar ratios are closed to the ones determined by XRF, suggesting that cerium is indeed added to zircon (Table 1). However, for the CC and the CI routes, we can observe that the Ce/Zr molar ratios calculated from XPS data are higher than the ones provided by XRF. Thus, in these cases we have an enrichment of the surface in cerium. However, the differences between Ce/Zr ratios determined by XPS and XRF are much smaller for the samples prepared from the CC route. When the other methods (AI, AI480) are used, both XRF and XPS results lead to a similar Ce/Zr molar ratio, suggesting a homogeneous distribution of cerium within the material and a higher degree of its incorporation in the zirconia network. From XPS results it is clear that impregnations on calcined (CI) or on amorphous (AI) mesostructured ZrO_2 lead to a higher oxygen content at the surface (Table 1). For example, for a targeted Ce/Zr molar ratio of 0.05, the oxygen content at the surface is 53.5 and 51.6 at.% for the mixed CeO_2-ZrO_2 oxides obtained by impregnation on the calcined and amorphous ZrO_2, respectively. This value is equal to 44.0 and 43.5 at.% for the $Ce_xZr_{1-x}O_2$ solid solutions obtained by the co-condensation method and after heating at 480°C of the samples obtained by impregnation on amorphous zirconia, respectively. Whatever the mixed oxide the bulk O/(Zr+Ce) ratio (≈ 1.8) determined by XRF (Table 2) is in the same range of order than the stoichiometry; i.e. 2. The surface one calculated from XPS varies from 2.2 to 2.7 (Table 1), the value greater than 2 can be due to adsorbed species such as water at the surface.

SEM-EDX and TEM-EDX analyses have been done on the 10 mol.% Ce materials (Fig. 3 and Fig. 4). From SEM-EDX elemental mappings the cerium appeared homogeneously dispersed when CC, AI and AI480 routes were followed for the preparation of the materials (Fig. 3A,B,C). However, the formation of large particles containing mainly Ce was observed for the material prepared by following the CI route (Fig. 3D). According to the XRD results these particles are CeO_2. TEM equipped with EDX analyzer has allowed to probe the element dispersion at higher magnification. Materials prepared by the CC route showed some areas rich in Ce (Fig. 4A) while a homogeneous dispersion of the Ce was observed for the materials prepared with AI and AI480 (Fig. 4B,C). Concerning the material prepared with the CI route small particles containing mainly Ce (Fig. 4D), most probably CeO_2 nanoparticles, were observed.

From the results reported above, it is obvious that the preparation method affects the dispersion of cerium on the mesostructured zirconia. When the ceria-zirconia oxides are obtained by impregnation on the calcined ZrO_2, even if we cannot completely exclude a partial diffusion of the cerium inside the zirconia framework, XRD, Raman, EDX and XPS results support the fact that CeO_2 particles are mainly formed at the surface of the mesostructured ZrO_2, whose walls are composed of a mixture of the tetragonal and monoclinic polymorphs of zirconia. When the cerium content reaches 10 mol.%, these ceria particles are clearly detected by Raman and XRD. We can assume that ceria is also present at the surface when the impregnation is carried out on the amorphous mesostructured zirconia. However, in this case since the calcination is limited to 300°C the growth of the ceria particles is limited and they are not detected by XRD or by Raman. They are relatively homogeneously dispersed at the surface of ZrO_2 as evidenced by EDX and by the high value of the Ce/Zr surface ratio calculated from XPS. Upon the further heating at 480 °C the diffusion of the cerium species into the bulk ZrO_2 occurs to form the $Ce_xZr_{1-x}O_2$ solid

solution, and as a consequence the Ce/Zr molar ratio at the surface decreases and the tetragonal structure of zirconia is stabilized by the incorporation of cerium into the ZrO_2 lattice. The $Ce_xZr_{1-x}O_2$ solid solution is also prepared by the co-condensation method through the EISA-derived method. During the evaporation of the solvent to form the hybrid mesophase, the hydrolyzed zirconium precursor and the cerium species can interact with the oxyethylene group of Pluronic P123. The cerium species are thus entrapped in the zirconia network. After surfactant removal by ethanol extraction the obtained material is heated at 480°C to induce the crystallization of the walls. During this step the cerium species can diffuse in the zirconia network to lead to the $Ce_xZr_{1-x}O_2$ solid solution as observed for the mixed oxides prepared by impregnation on the amorphous zirconia followed by a heating at 480°C. However, in the case of the compounds synthesized through the co-condensation route, with the increase of the cerium content its repartition becomes less homogenous as observed by EDX, which reveal the presence of area enriched in cerium. This is also reflected by the Ce/Zr surface ratio that is slightly higher than the bulk one (0.11 against 0.08).

3.3. Catalytic oxidation of toluene using mesostructured CeO_2-ZrO_2 materials

3.3. Catalytic oxidation of toluene using mesostructured CeO_2-ZrO_2 materials

After characterization, the mixed oxides have been used as catalysts for the toluene oxidation. The curves giving the selectivities into CO_2 and CO, the only by-product detected, are found in Figure S8. No CO formation is observed for pure CeO_2 whereas several ppm of CO are formed during the light off curves for the samples containing ZrO_2. The toxic emission of CO could be easily avoided by a slight impregnation of copper or cobalt on the samples[53,54]. Introduction of copper will be the subject of future work and in this case, we will also perform H_2-TPR characterization on the CeO_2-ZrO_2 mesostructured materials with copper to find a correlation between the physicochemical properties of the catalysts and their catalytic activity.

The CO_2 content (Fig. S8A) slightly above the theoretical value can be explained by some desorption of CO_2 adsorbed at lower temperature on the material. This is often found with the light off curve method. The evolution of the conversion rate as a function of both the cerium content and the preparation method is depicted in Figure 5. Catalytic results have been compared with the ones obtained using a commercial non-mesostructured CeO_2 having an interparticular porosity with a specific surface area of 79 m²/g. Values of the maximal conversion rate and of T_{50}, temperature at which 50% conversion of toluene is achieved, are given in Table 2. From the T50 (°C) values listed in Table 2, it is clear that an increase of Ce content whatever the mode of preparation of the catalyst increases the catalytic efficacy. Indeed, the conversion rate of toluene increases as a function of the cerium content. The same tendency was also found for De Rivas and coll[55] on a series of $Ce_xZr_{1-x}O_2$ for toluene oxidation. If we compare the mode of preparation by the 10 mol.% CeO_2 catalysts, the order of catalytic activity given by T50 is as follows: CI > AI480 > AI > CC. The series of materials studied have different specific surface areas. In order to standardize the parameters affecting the catalytic performance, the correlations should be made taking into account the specific activity. The formula used therefore takes into consideration the specific surface area and the mass of catalyst used. For the oxidation of toluene, previous work has shown a kinetic order of 1 for toluene[56]. The applied activity formula is therefore characteristic of a first order reaction and is calculated at low conversion (10%). The specific and intrinsic activities of the catalysts prepared in the presence of 10 mol.% of cerium have been compared to the one of the commercial CeO_2, used as reference (Table 3). The same activity order is actually found according to the more precise specific or intrinsic activities (Table 3). The comparison of the intrinsic activities which takes the specific surface into account shows that the specific surface does not play a crucial role in the performance of the catalyst. This observation is currently found in the literature for VOC oxidation. However, it could play a role for the dispersion of a

deposited phase. According to this classification, high surface Ce quantity implies a high catalytic activity. In fact, when the Ce^{4+}/Ce^{3+} ratio but also the oxygen content at the surface (given by XPS), the catalytic efficiency increases. The work of Zhou and coll[57] on MnOx / CeO_2-ZrO_2 catalysts showed that on catalysts where the quantity of Ce^{4+} (or Ce^{4+}/Ce^{3+}) at the surface (XPS data) was the greatest, the activity for oxidation of toluene was also greatest at low temperature. They also showed that activity was also linked to a greater amount of Ce on the surface. On the other hand, a solid solution prepared by the coprecipitation method[58] does not perform well in the oxidation of VOCs without an active deposited phase. In addition, this solid solution is also less efficient (only cubic phase) than a zirconia-ceria sample also having the tetragonal phase[57].

Therefore, a better oxidation of toluene is found on the mixed CeO_2-ZrO_2 oxides obtained by impregnation on the calcined (CI) or amorphous ZrO_2 (AI) than on the $Ce_xZr_{1-x}O_2$ solid solutions obtained by the co-condensation method (CC) or after heating at 480°C of the samples obtained by impregnation on amorphous zirconia (AI480).

4. Conclusions

In this study, to investigate the effect of the preparation method of nanostructured mixed ZrO_2-CeO_2 oxides on the toluene oxidation, materials have been synthesized by either co-precipitation of cerium and zirconium precursors using an EISA-derived route or by wet impregnation on nanostructured zirconia using cerium acetate. The wet impregnation has been carried out on semi-crystalline nanostructured ZrO_2, previously calcined at 480°C and on amorphous zirconia followed or not by a heating at 480°C. A better dispersion of cerium and a stabilization of the tetragonal structure are noted when the mixed oxides are prepared from the co-condensation or the wet impregnation on amorphous mesostructured ZrO_2 followed by a heating at 480°C. In addition, XPS data show that there is no enrichment of the surface in

cerium. This is not the case when the impregnation is carried out on a semi-crystalline mesostructured ZrO_2, which has been previously calcined at 480°C. Indeed, XRD, TEM-EDX and SEM-EXD reveal the presence of nano sized ceria particles. Using this preparation route, the repartition of cerium is thus less homogeneous. A mixture of monoclinic and tetragonal structures is also observed by XRD and Raman spectroscopy.

Then, the activity of the mixed oxides has been evaluated for the oxidation of toluene, which is a probe VOC molecule. Results show that the bare ZrO_2 material is almost not active for the total oxidation of toluene. Regarding the CeO_2-ZrO_2 supports, it appears that the preparation method strongly affects the toluene conversion. The solid solution containing 10 mol.% of cerium and prepared by impregnation on amorphous nanostructured ZrO_2 followed by a heating at 480 °C exhibits the highest conversion of toluene and is almost as efficient as pure commercial ceria. For this sample, the Ce/Zr and the Ce^{4+}/Ce^{3+} surface ratios found by XPS are higher than for the other catalysts. Moreover, low amounts of CO are formed during the reaction when ZrO_2 based materials are used as catalysts. However, the production of CO during the reaction can be completely inhibited by dispersing copper on the CeO_2-ZrO_2 nanostructured material. This work is under progress.

Conflicts of interest

The authors declare that they have no competing interests

Acknowledgments

We would like to thank the platform “Spectroscopies et Microscopies des Interfaces” and Aurélien Renard (LCPME) for XPS analyses. The platforms “X-ray diffraction”, “Electronic microscopy” and “Spectroscopies FTIR and Raman” of IS2M are also acknowledged. Florian

Jonas thanks the « Region Grand-Est » for the financial support of his PhD [grant number RPHPHXAS-D-AOT17-TITAN].

Funding:

This work was supported by the « Region Grand-Est » [grant number RPHPHXAS-D-AOT17-TITAN].

Supporting information

Textural parameters of the CeO_2-ZrO_2 nanoporous oxides (Table S1).

Variation of the position of the (101) reflection of the tetragonal phase as a function of the targeted cerium content (S1).

Evolution of the Raman spectra as a function of the targeted cerium content (S2)

SAXS patterns as a function of the targeted cerium content (S3).

TEM images of samples prepared in the presence of 10 mol.% of Ce (S4).

Evolution of the nitrogen adsorption/desorption isotherms as a function of the targeted cerium content (S5).

Evolution of the mesopores size distribution as a function of the targeted cerium content (S6).

Zr 3d and O 1s XPS spectra of the CeO_2/ZrO_2 material prepared by impregnation on amorphous ZrO_2 (S7).

Evolution of CO_2 (A) and CO (B) content as a function of the targeted cerium content (S8).

References

1 Inoue, Y.; Yamazaki, H. Studies of the Hydrous Zirconium(IV) Oxide Ion Exchanger. I. Ion-Exchange Properties and Effect of Heat Treatment. *Bull. Chem. Soc. jpn.*, **1987**, *60*, 891-897.

2 Srinivasan, R.; Davis, B.H. In: Materials Synthesis and Characterization; Perry, D.L., Ed; Springer Science+Business Media: New York, 1997, pp. 147-188.

3 Zhang, C. Tunable Luminescence in Monodisperse Zirconia Spheres. *Langmuir*, **2009**, *25*, 7078-7083.

4 Corma, A. From Microporous to Mesoporous Molecular Sieve Materials and Their Use in Catalysis. *Chem. Rev.*, **1997**, *97*, 2373-2420.

5 Lin, J.; Song, H.; Shen, X.; Wang, B.; Xie, S.; Deng, W.; Wu, D.; Zhang, Q.; Wang, Y. Zirconia-supported rhenium oxide as an efficient catalyst for the synthesis of biomass-based adipic acid ester. *Chem. Commun.*, **2019**, *55*, 11017-11020.

6 Cai, Q.; Lopez-Ruiz, J.A.; Cooper, A.R.; Wang, J.G.; Albrecht, K.O.; Mei, D. Aqueous-Phase Acetic Acid Ketonization over Monoclinic Zirconia. *ACS Catal.*, **2018**, *8*, 488-502.

7 Trovarelli, A. Catalytic Properties of Ceria and CeO_2-Containing Materials, *Catal. Rev.*, **1996**, *38*, 439-520.

8 Montini, T.; Melchionna, M.; Monai, M.; Fornasierao, P. Dundamentals and Catalytic Applications of CeO_2-Based Materials, *Chem. Rev.*, **2016**, *116*, 5987-6041.

9 *Catalysis by Ceria and Related Materials*, Trovarelli, A.; Fornasierao, P., Eds, Hutchings, Series Ed; Imperial College Press: London, 2013.

10 Devaiah, D.; Reddy, L.H.; Park, S.E.; Reddy, B.M. Ceria–Zirconia Mixed Oxides: Synthetic Methods and Applications*, Catal. Rev. Sci. Eng.*, **2018**, *60*, 177-277.

11 Li, J.; Liu, H.; Deng, Y.; Liu, G.; Chen, Y. ; Yang, J. Emerging Nanostructured Materials for the Catalytic Removal of Volatile Organic Compounds. *Nanotechnol. Rev.*, **2016**, *5*, 147-181.

12 Topka, P.; Kaluža, G., Total Oxidation of Ethanol and Toluene over Ceria–Zirconia Supported Platinum Catalysts. *Chem. Pap.*, **2016**, *70*, 898-906.

13 Tsoncheva, T.; Ivanova, R.; Henych, J.; Dimitrov, M.; Kormunda, M.; Kovacheva, D.; Scotti, N.; Dal Santo, V.; Štengl, V. Effect of Preparation Procedure on the formation of Nanostructured Ceria–Zirconia Mixed Oxide catalysts for Ethyl Acetate Oxidation: Homogeneous Precipitation with Urea vs Template-Assisted Hydrothermal Synthesis. *Appl. Catal., A*, **2015**, *505*, 418-432.

14 Ozawa, M.; Yuzuriha, H.; Haneda, M. Total Oxidation of Toluene and Oxygen Storage Capacity of Zirconia-Sol Modified Ceria Zirconia. *Catal. Commun.*, **2013**, *30*, 32-35.

15 Idakiev, V.; Dimitrov, D.; Tabakova, T.; Ivanov, K.; Yuan, Z.Y.; Su, B.L. Catalytic Abatement of CO and Volatile Organic Compounds in Waste Gases by Gold Catalysts Supported on Ceria-Modified Mesoporous Titania and Zirconia. *Chin. J. Catal.*, **2015**, *36*, 579-587.

16 Piumetti, M.; Bensaid, S.; Fino, D.; Russo, N. Nanostructured Ceria-Zirconia Catalysts for CO Oxidation: Study on Surface Properties and Reactivity. *Appl. Catal., B*, **2016**, *197*, 35-46.

17 Pudukudy, M.; Yaakob, Z. Catalytic Aspects of Ceria-Zirconia Solid Solution: Part-I An Update in the Synthesis, Properties and Chemical Reactions of Ceria Zirconia Solid Solution. *Der Pharma Chemica*, **2014**, *6*, 224-240.

18 Carbajal-Ramos, I.A.; Andrade-Gamboa, J.; Gennari, F.C. Nanostructured $Ce_{1-x}Zr_xO_2$ Solid Solutions Produced by Mechanochemical Processing. *Mater. Chem. Phys.*, **2013**, *137*, 1073-1080.

19 Pudukudy, M.; Yaakob, Z.; Narayanan, B. Selective Vapour Phase Oxidation of Benzyl Alcohol to Benzaldehyde over Mesoporous Ceria–Zirconia Solid Solution Synthesized Via a Facile Citrate Route. *J. Clust. Sci.*, **2014**, *25*, 1599-1614.

20 Sellick, D.R.; Aranda, A.; García, López, J.M.; Solsona, B. ; Mastral, A.M.; Morgan, D.J.; Carley, A.F.; Taylor, S.H. Influence of the Preparation Method on the Activity of Ceria Zirconia Mixed Oxides for Naphthalene Total Oxidation. *Appl. Catal., B*, **2013**, *132-133*, 98-106.

21 Huang, W.; Yang, J.; Wang, W.; Zou, B.; Meng, X.; Wang, Y. ; Cao, X. ; Wang, Z. Effects of Zr/Ce Molar Ratio and Water Content on Thermal Stability and Structure of ZrO_2–CeO_2 Mixed Oxides Prepared via Sol–Gel Process. *Mater. Res. Bull.*, **2012**, *47*, 2349-2356.

22 Rumruangwong, M.; Wongkasemjit, S. Synthesis of Ceria–Zirconia Mixed Oxide from Cerium and Zirconium Glycolates via Sol–Gel Process and its Reduction Property. *Appl. Organometal. Chem.*, **2006**; *20*, 615-625.

23 Kaminski, P.; Ziolek, M.; Van Bokhoven, J.A. Mesoporous Cerium-Zirconium Oxides Modified with Gold and Copper - Synthesis, Characterization and Performance in Selective Oxidation of Glycerol. *RSC Adv.*, **2017**, *7*, 7801-7819.

24 Yang, X.; Cheng, X.; Ma, J.; Zou, Y.; Luo, W.; Deng, Y. Large-Pore Mesoporous CeO_2-ZrO_2 Solid Solutions with In-Pore Confined Pt Nanoparticles for Enhanced CO Oxidation. *Small*, **2019**, 1903058.

25 Barakat, T.; Rooke, J.C.; Tidahy, H.L.; Hosseini, M.; Cousin, R.; Lamonier, J.F.; Giraudon, J.M.; De Weireld, G.; Su, B.L.; Siffert, S. Noble-Metal-Based Catalysts

Supported on Zeolites and Macro-Mesoporous Metal Oxide Supports for the Total Oxidation of Volatile Organic Compounds. *ChemSusChem*, **2011**, **4**, 1420-1430.

26 Li, W.; Wu, Z.; Wang, J.; Elzatahry, A.A.; Zhao, D. A Perspective on Mesoporous TiO_2 Materials. *Chem. Mater.*, **2014**, *26*, 287-298.

27 Peng, Y.; Shiyu, Z.; Jiaheng, L. Preparation of Ordered Mesoporous Nanocrystalline Ceria and Ceria-zirconia for Soot Oxidation. *J. Wuhan Univ. Technol.-Mat. Sci. Edit.*, **2016**, *31*, 113-117.

28 Kimura, T. Evaporation-induced Self-assembly Process Controlled for Obtaining Highly Ordered Mesoporous Materials with Demanded Morphologies. *Chem. Rec.* **2016**, *16*, 445-457.

29 Brezesinski, T.; Antonietti, M.; Groenewolt, M.; Pinna, N.; Smarsly, B. The Generation of Mesostructured Crystalline CeO_2, ZrO_2 and CeO_2-ZrO_2 Films using Evaporation-Induced Self-assembly. *New J. Chem.*, **2005**, *29*, 237-242.

30 Zou, Y.; Zhou, X.; Ma, J.; Yang, X.; Deng, Y. Recent Advances in Amphiphilic Block Copolymer Templated Mesoporous Metal-Based Materials: Assembly Engineering and Applications. *Chem. Soc. Rev.*, **2020**, *49*, 1173-1208.

31 Li, C.; Gu, X.; Wang, Y.; Wang, Y.; Wang, Y.; Liu, X.; Lu, G. Synthesis and Characterization of Mesostructured Ceria-Zirconia Solid Solution. *J. Rare Earths*, **2009**, *27*, 211-215.

32 Barroso-Bogeat, A.; Núñez-Pérez, B.; Blanco, G.; Pintado, J.M. ; Hermández-Garrido, J.C.; Calvino, J.J. Surface and Redox Characterization of New Nanostructured ZrO_2@CeO_2 Systems with Potential Catalytic Applications. *Surf. Interface Anal.*, **2018**, *50*, 1025-1029.

33 Cabeza, I; Souto, L.G.; Pintado, J.M.; Pereira, C.; Freire, C.; Blanco, G. Influence of Ceria Distribution on the Redox Behaviour of Nanoparticulated CeO_2-SiO_2 Systems withA in Catalysis. *Surf. Interface Anal.*, **2014**, *46*, 712-715.

34 Pilar Yeste, M.; Hernández-Garrido, J.C.; Carolina Arias, D.; Blanco, G.; Rodríguez-Izquierdo, J.M.; Pintado, J.M.; Bernal, S.; Pérez-Omil, J.A.; Calvino, J.J. Rational Design of Nanostructured, Noble Metal Free, Ceria–Zirconia Catalysts with Outstanding Low Temperature Oxygen Storage Capacity. *J. Mater. Chem. A*, **2013**, *1*, 4836-4844.

35 Lebeau, B.; Naboulsi, I. ; Michelin, L. ; Marichal, C. ; Rigolet, S. ; Carteret, C. ; Brunet, S. ; Bonne, M. ; Blin, J.L. Amorphous Mesostructured Zirconia with High (Hydro)Thermal Stability. *RSC Adv.*, **2020**, *10*, 26165-26176.

36 Ding, S.; Zhao, J.; Yu, Q. Effect of Zirconia Polymorph on Vapor-Phase Ketonization of Propionic Acid. *Catalysts*, **2019**, *9*, 768.

37 Wang, G.; Meng, F.; Ding, C.; Chu, P.K.; Liu, X. Microstructure, Bioactivity and Osteoblast Behavior of Monoclinic Zirconia Coating with Nanostructure Surface. *Acta Biomater.*, **2010**, *6*, 990-1000.

38 Haynes, W.M.; Lide, D.R.; Bruno, T.J. In: CRC Handbook of Chemistry and Physics, 97th ed., CRC Press, Taylor & Francis Group, Boca Raton, FL, 2016-2017, pp 12-12.

39 Li, P.; Chen, I.W. Effect of Dopants on Zirconia Stabilization-An X-ray Absorption Study: II, Tetravalent Dopants. *J. Am. Chem. Soc.*, **1994**, *77*, 1281-1288.

40 Bechepeche, A.P.; Treu, O.; Longo, Jr. E.; Paiva-Santos, C.O.; Varela, J.A. Experimental and Theoretical Aspects of the Stabilization of Zirconia. *J. Mater. Sci.*, **1999**, *34*, 2751-2756.

41 Mastealaro, V.R.; Briois, V.; De Souza, D.P.F.; Silva, C.L. Structural Studies of a ZrO_2-CeO_2 doped system. *J. Eur. Ceram. Soc.*, **2003**, *23*, 273-282.

42 Savin, A.; Craus, M.L.; Turchenko, V.; Bruma, A.; Dubos, P.A.; Malo, S.; Konstantinova, T.E.; Burkhovetsky, V.V. Monitoring Techniques of Cerium Stabilized Zirconia for Medical Prosthesis. *Appl. Sci.*, **2015**, *5*, 1665-1682.

43 Chatterjee, A.; Pradhan, S.K.; Datta, A.; De, M.; Chakravorty, D. Stability of Cubic Phase in Nanocrystalline ZrO_2. *J. Mater. Res.*, **1994**, *9*, 263-265.

44 Martínez-Arias, A.; Fernández García, M.; Ballesteros, V. ; Salamanca, L.N. ; Conesa, J.C. ; Otero, C. ; Soria, J. Characterization of High Surface Area Zr-Ce (1 :1) Mixed Oxide Prepared by a Microemulsion Method. *Langmuir*, **1999**, *15*, 4796-4802.

45 López, E.F.; Escribano, V.S.; Panizza, M.; Carnasciali, M.M.; Busca, G. Vibrational and Electronic Spectroscopic Properties of Zirconia Powders. *J. Mater. Chem.*, **2001**, *11*, 1891-1897.

46 Bagshaw, S.A.; Prouzet, E.; Pinnavaia, T.J. Templating of Mesoporous Molecular Sieves by Nonionic Polyethylene Oxide Surfactants. *Science*, **1995**, *269*, 1242-1244.

47 Sing, K.S.W.; Everett, D.H.; Haul, R.A.W.; Moscou, L.; Pierotti, R.A.; Rouquerol, J.; Siemieniewska, T. Reporting Physisorption Data for Gas/Solid Systems with Special Reference to the Determination of Surface Area and Porosity (Recommendations 1984). *IUPAC, Pure Appl. Chem.*, **1985**, *57*, 603-619.

48 Bêche, E.; Charvin, P.; Perarnau, D.; Abanades, S.; Flamant, G. Ce 3d XPS Investigation of Cerium Oxides and Mixed Cerium Oxide (CexTiyOz). *Surf. Interface Anal.*, **2008**, *40*, 264-267.

49 Burroughs, P.; Hamnett, A.; Orchard, A.F.; Thornton, G. J. Satellite structure in the X-Ray Photoelectron Spectra of Some Binary and Mixed Oxides of Lanthanum and Cerium. *Chem. Soc., Dalton Trans.*, **1976**, *17*, 1686-1698.

50 Worn Park, P.; Ledford, J.S. Effect of Crystallinity on the Photoreduction of Cerium Oxide: A Study of CeO_2 and Ce/Al_2O_3 Catalysts. *Langmuir* **1996**, *12*, 1794-1799

51 Gondal, M.A.; Fasasi, T.A.; Baig, U.; Mekki, A. Effect of Oxidizing Media on the Composition, Morphology and Optical Properties of Colloidal Zirconium Oxide Nanoparticles Synthesized via Pulsed Laser Ablation in Liquid Technique. *J. Nanosci. Nanotechnol.*, **2018**, *18*, 1030-4039.

52 Galtayries, A.; Sporken, R.; Riga, J.; Blanchard, G.; Caudano, R. XPS Comparative Study of Ceria/Zirconia Mixed Oxides: Powders and Thin Film Characterization. *J. electron spectrosc. relat. phenom.*, **1998**, *88-91*, 951-956.

53 Labaki M., Siffert S., Lamonier J.-F., Zhilinskaya E.A., Aboukaïs A. Total Oxidation of Propene and Toluene in the Presence of Zirconia Doped by Copper and Yttrium: Role of Anionic Vacancies. *Appl. Catal. B Env.* **2003**, *43(3)*, 261-271.

54 Dib H., El Khawaja R., Rochard G., Poupin C., Siffert S., Cousin R. CuAlCe Oxides Issued from Layered Double Hydroxide Precursors for Ethanol and Toluene Total Oxidation. *Catalysts* **2020**, *10(8)*, 870.

55 De Rivas B., Jose I. Gutierrez-Ortiz J.I., Lopez-Fonseca R., Gonzalez-Velasco J. R. *Appl. Catal. A* **2006**, 314, 54–63

56 Genty E., Siffert S., Cousin R. Kinetic Modelling for the Toluene Total Oxidation in Presence of CoAlCe Catalyst. *Catal. Today* **2019**, 333, 28-35.

57 Zhou C., Zhang H., Zhang Z., Li L.; *Appl. Surf. Sci.* **2021**, 539, 148-188

58 Hou Z., Feng J., Lin T., Zhang H., Zhou X., Chen Y., *Appl. Surf. Sci.* **2018**, 434, 82–90

Figures caption

Scheme 1: Schematic representation of the different routes used to prepare the Nanoporous CeO_2-ZrO_2 mixed oxides.

Figure 1: Evolution of the X-ray diffractograms as a function of the targeted cerium content. Materials have been prepared by co-condensation (A), or by impregnation on mesostructured ZrO_2 calcined at 480°C (B), on amorphous mesostructured ZrO_2 (C) and on amorphous mesostructured ZrO_2 followed by a heating at 480°C (D). * correspond to CeO_2 reflections.

Figure 2: Ce 3d XPS spectrum of the CeO_2/ZrO_2 oxides prepared in the presence of 5 mol.% of cerium. Materials have been prepared by co-condensation (A), or by impregnation on mesostructured ZrO_2 calcined at 480°C (B), on amorphous mesostructured ZrO_2 (C) and on amorphous mesostructured ZrO_2 followed by a heating at 480°C (D).

Figure 3: SEM images and EDX Zr, Ce elemental mappings of materials prepared by co-condensation (A), by impregnation on amorphous mesostructured ZrO_2 (B), by impregnation on amorphous mesostructured ZrO_2 followed by a heating at 480°C (C), and by impregnation on mesostructured ZrO_2 calcined at 480°C (D)

Figure 4: TEM images and EDX Zr, Ce elemental mappings of materials prepared by co-condensation (A), by impregnation on amorphous mesostructured ZrO_2 (B), by impregnation on amorphous mesostructured ZrO_2 followed by a heating at 480°C (C), and by impregnation on mesostructured ZrO_2 calcined at 480°C (D). *Red arrows indicate nanoparticles with Ce major content.*

Figure 5: Toluene conversion as a function of the targeted cerium content. Materials have been prepared by co-condensation (A), or by impregnation on mesostructured ZrO_2 calcined at 480°C (B), on amorphous mesostructured

ZrO_2 (C) and on amorphous mesostructured ZrO_2 followed by a heating at 480°C (D).

Table 1: Oxygen, zirconium, cerium contents, Ce/Zr molar ratio, Ce^{4+}/Ce^{3+} ratio and O/(Ce+Zr) ratio obtained from XPS and/or XRF analyzes.

	XPS							XRF		
	Targeted Ce/Zr molar ratio	O (at.%)	Zr (at.%)	Ce (at.%)	Ce/Zr molar ratio	Ce^{4+}/Ce^{3+} ratio	O/(Zr+ Ce) ratio	Zr (mol.%)	Ce (mol.%)	Ce/Zr molar ratio
CC	0.03	44.9	18.5	0.4	0.02	0.6	2.4	32.5	0.8	0.02
	0.05	44.0	18.3	1.0	0.05	0.9	2.3	32.2	1.1	0.04
	0.11	42.4	16.3	1.9	0.11	1.8	2.3	30.6	2.6	0.08
CI	0.01	51.0	21.2	1.4	0.06		2.3	32.9	0.3	0.01
	0.03	49.4	19.2	1.3	0.07	1.1	2.4	32.3	0.8	0.03
	0.05	53.5	20.7	2.6	0.12	1.4	2.3	31.8	1.4	0.04
	0.11	51.2	18.4	4.6	0.25	2.2	2.2	30.3	2.9	0.10
AI	0.01	50.0	19.3	0.3	0.01		2.6	32.8	0.2	0.01
	0.03	51.0	20.0	0.6	0.03		2.5	31.9	0.9	0.03
	0.05	51.6	18.9	1.2	0.06	1.1	2.6	32.2	1.1	0.03
	0.11	54.9	17.7	2.7	0.15	1.0	2.7	29.1	4.2	0.14
AI480	0.03	44.2	18.0	0.5	0.03	0.4	2.4	31.9	0.9	0.03
	0.05	43.5	17.9	0.7	0.04	0.7	2.3	32.2	1.1	0.03
	0.11	41.6	16.2	2.4	0.15	0.6	2.2	29.1	4.2	0.14

CC: Materials prepared by the co-condensation method.
CI : Materials prepared by the impregnation on the mesostructured ZrO_2 calcined at 480°C.
AI: Materials prepared by the impregnation on the amorphous mesostructured ZrO_2.
AI480 : Materials prepared by the impregnation on the amorphous mesostructured ZrO_2 followed by a heating at 480°C.

Table 2: Maximum conversion rate (τ_{max}) at 400°C and temperature at which 50% conversion of toluene is achieved (T_{50}) as a function of the Ce amount (mol.%) and of the preparation method

Preparation method	Targeted % Ce (mol.%)	τ_{max}	T_{50} (°C)
CC	0	4	-
	1	9	-
	5	36	-
	10	74	317
CI	0	4	-
	1	54	345
	5	96	282
	10	96	263
AI	0	4	-
	1	16	-
	5	49	350
	10	72	294
AI480	0	4	-
	1	16	-
	5	22	-
	10	84	289
Commercial CeO_2		89	232

CC: Materials prepared by the co-condensation method.
CI : Materials prepared by the impregnation on the mesostructured ZrO_2 calcined at 480°C.
AI: Materials prepared by the impregnation on the amorphous mesostructured ZrO_2.
AI480 : Materials prepared by the impregnation on the amorphous mesostructured ZrO_2 followed by a heating at 480°C.

Table 3: Maximum conversion rate (τ_{max}), temperature at which 50% conversion of toluene is achieved (T_{50}) , specific activity (Γ_a) and intrinsic activity ($\Gamma_{intrinsic}$) at T_{10} of the mixed oxides prepared in the presence of 10 mol.% of cerium and of the commercial CeO_2 used as reference. T_{10} is the temperature at which the conversion rate of toluene is equal to 10%.

Catalyst	τ_{max}	T_{50} (°C)	T_{10} (°C)	S_{BET} (m^2/g)	Γ_a (10^{-8} mol/g.s^{-1})	$\Gamma_{intrinsic}$ (10^{-10} mol/m^2.s^{-1})
CeO_2	89.3	232	156	79	4.0	5.1
CC	73.7	313	268	172	3.5	2.0
CI	96.2	256	220	149	3.9	2.6
AI	71.5	294	252	238	3.6	1.5
AI480	84.1	289	244	160	3.8	2.4

CC: Mixed oxide prepared by the co-condensation method.
CI : Mixed oxide by the impregnation on the mesostructured ZrO_2 calcined at 480°C.
AI: Mixed oxide prepared by the impregnation on the amorphous mesostructured ZrO_2.
AI480 : Mixed oxide prepared by the impregnation on the amorphous mesostructured ZrO_2 followed by a heating at 480°C.

Scheme 1

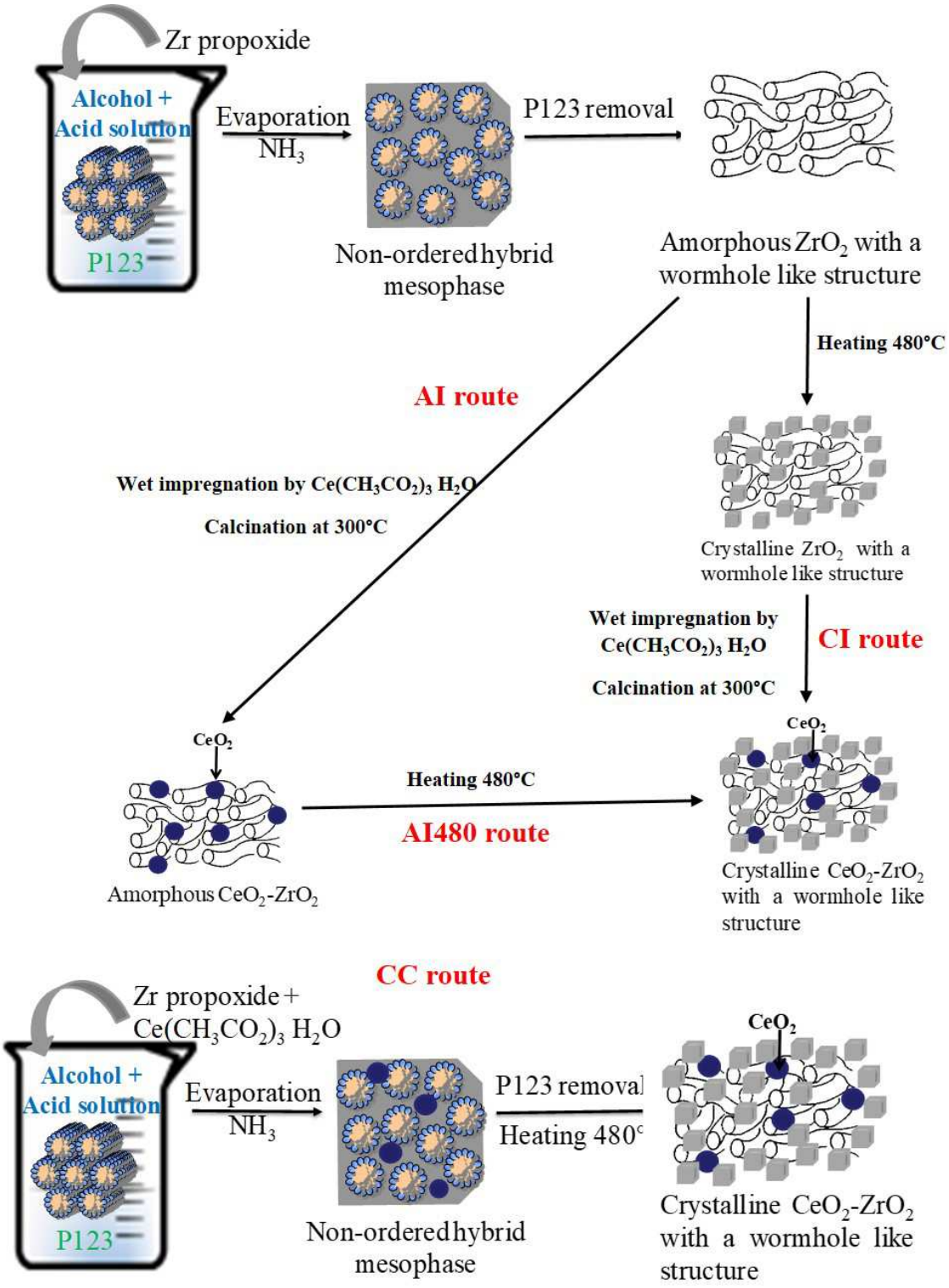
Zr propoxide
Alcohol + Acid solution
P123
Evaporation
NH3
Non-ordered hybrid mesophase
P123 removal
Amorphous ZrO2 with a wormhole like structure
Heating 480°C
AI route
Wet impregnation by Ce(CH3CO2)3 H2O
Calcination at 300°C
Crystalline ZrO2 with a wormhole like structure
Wet impregnation by Ce(CH3CO2)3 H2O
Calcination at 300°C
CI route
CeO2
Heating 480°C
AI480 route
Amorphous CeO2-ZrO2
Crystalline CeO2-ZrO2 with a wormhole like structure
CC route
Zr propoxide + Ce(CH3CO2)3 H2O
Alcohol + Acid solution
P123
Evaporation
NH3
Non-ordered hybrid mesophase
P123 removal
Heating 480°C
CeO2
Crystalline CeO2-ZrO2 with a wormhole like structure

Figure 1

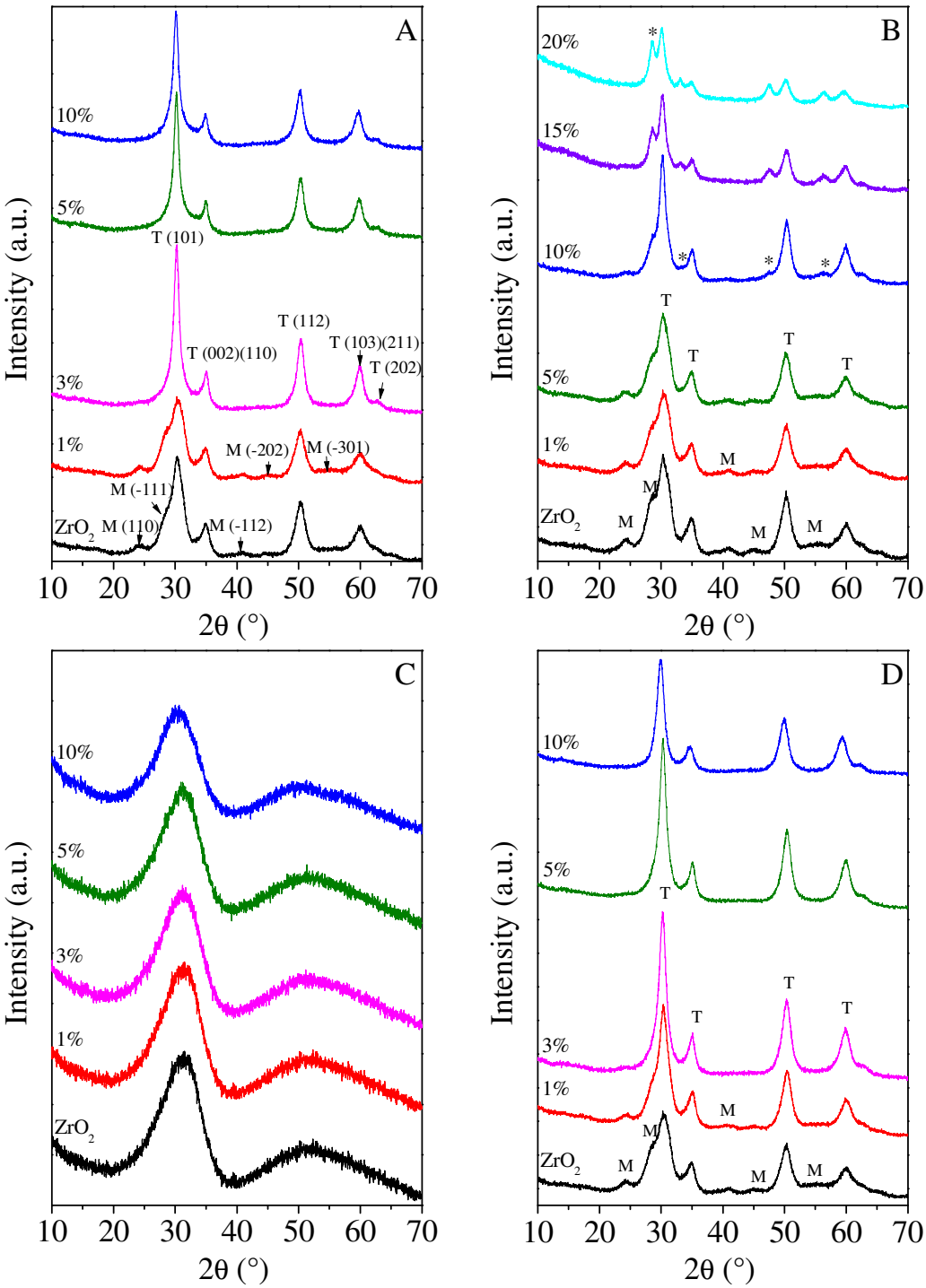
A
10%
5%
T (101)
3%
T (002)(110)
T (112)
T (103)(211)
T (202)
1%
M (-202)
M (-301)
M (-111)
ZrO2
M (110)
M (-112)
Intensity (a.u.)
10 20 30 40 50 60 70
2θ (°)
B
20%
15%
10%
5%
1%
ZrO2
M
T
C
10%
5%
3%
1%
ZrO2
D
10%
5%
3%
1%
ZrO2

Figure 2

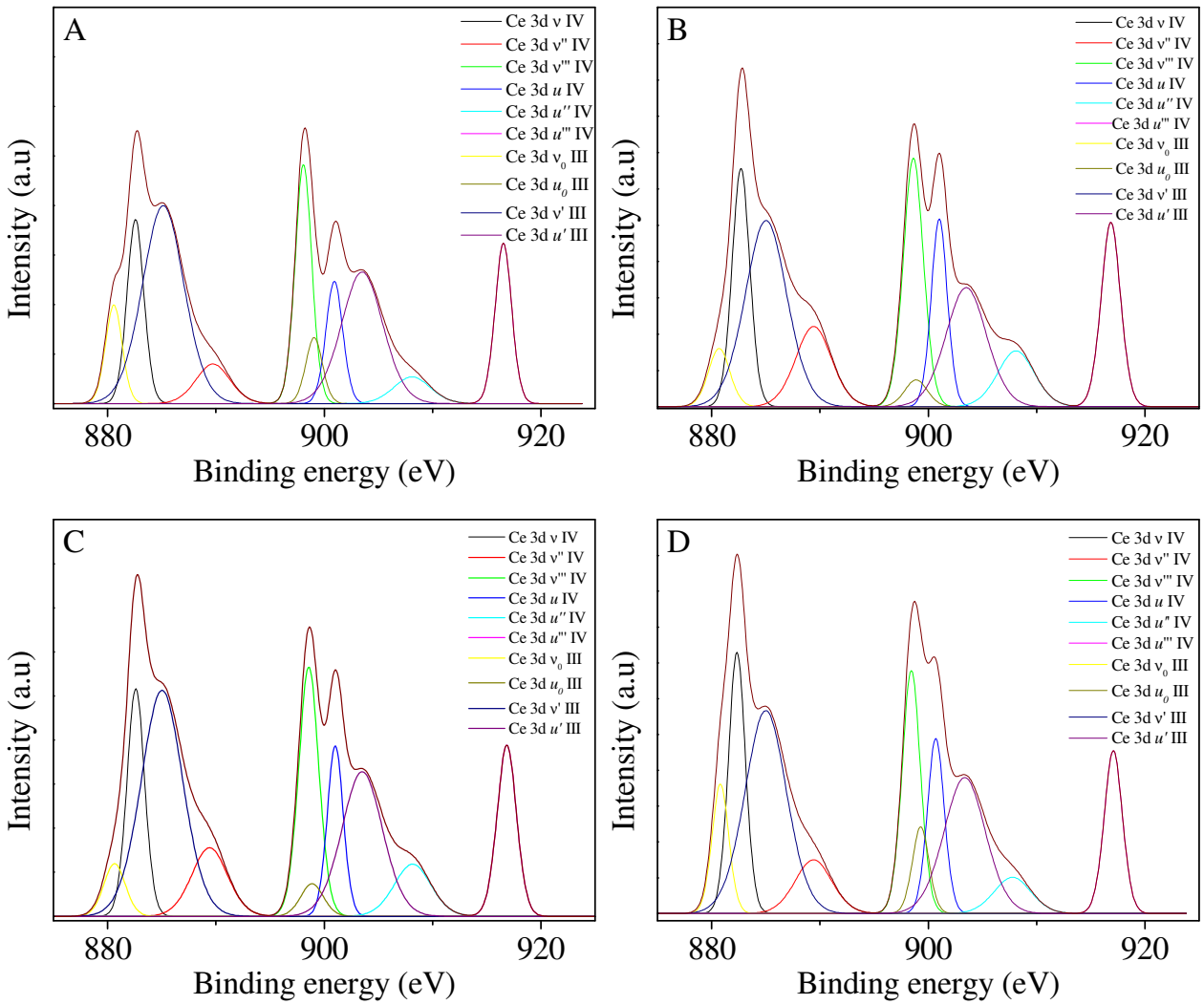
A
B
C
D
Ce 3d v IV
Ce 3d v'' IV
Ce 3d v''' IV
Ce 3d u IV
Ce 3d u'' IV
Ce 3d u''' IV
Ce 3d v0 III
Ce 3d u0 III
Ce 3d v' III
Ce 3d u' III
Intensity (a.u)
880
900
920
Binding energy (eV)

Figure 3

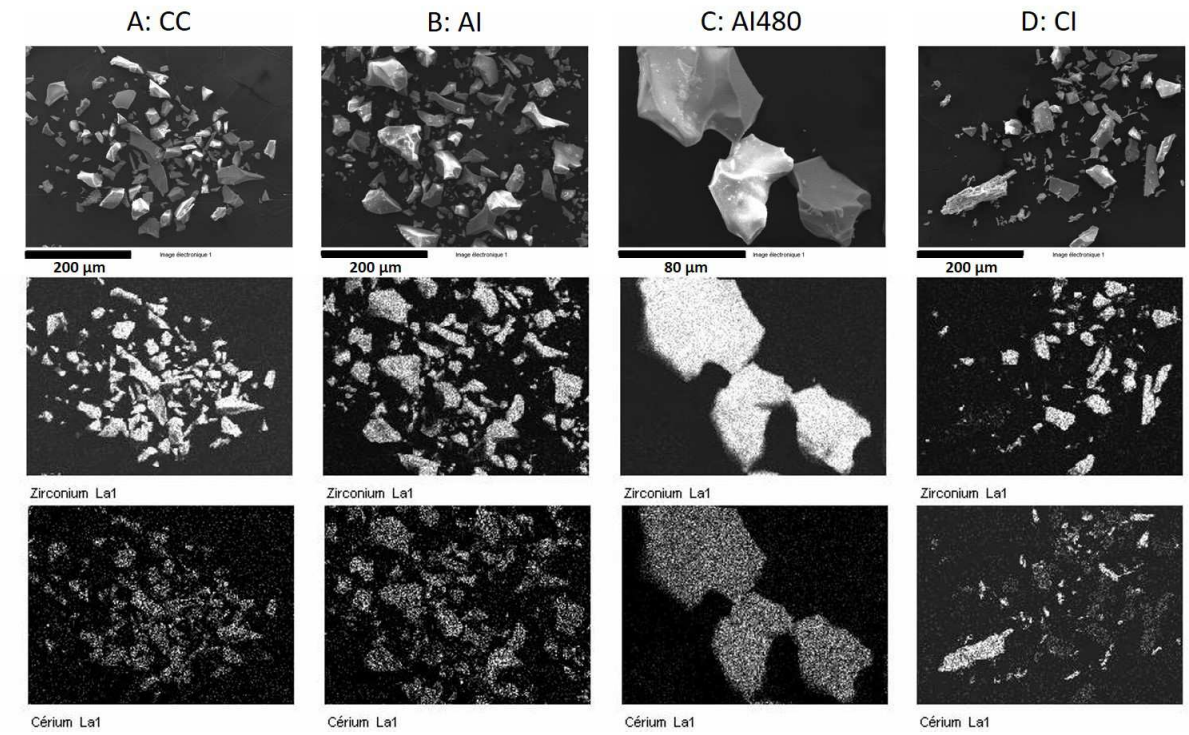
A: CC
B: Al
C: Al480
D: Cl
200 µm
200 µm
80 µm
200 µm
Zirconium La1
Zirconium La1
Zirconium La1
Zirconium La1
Cérium La1
Cérium La1
Cérium La1
Cérium La1

Figure 4

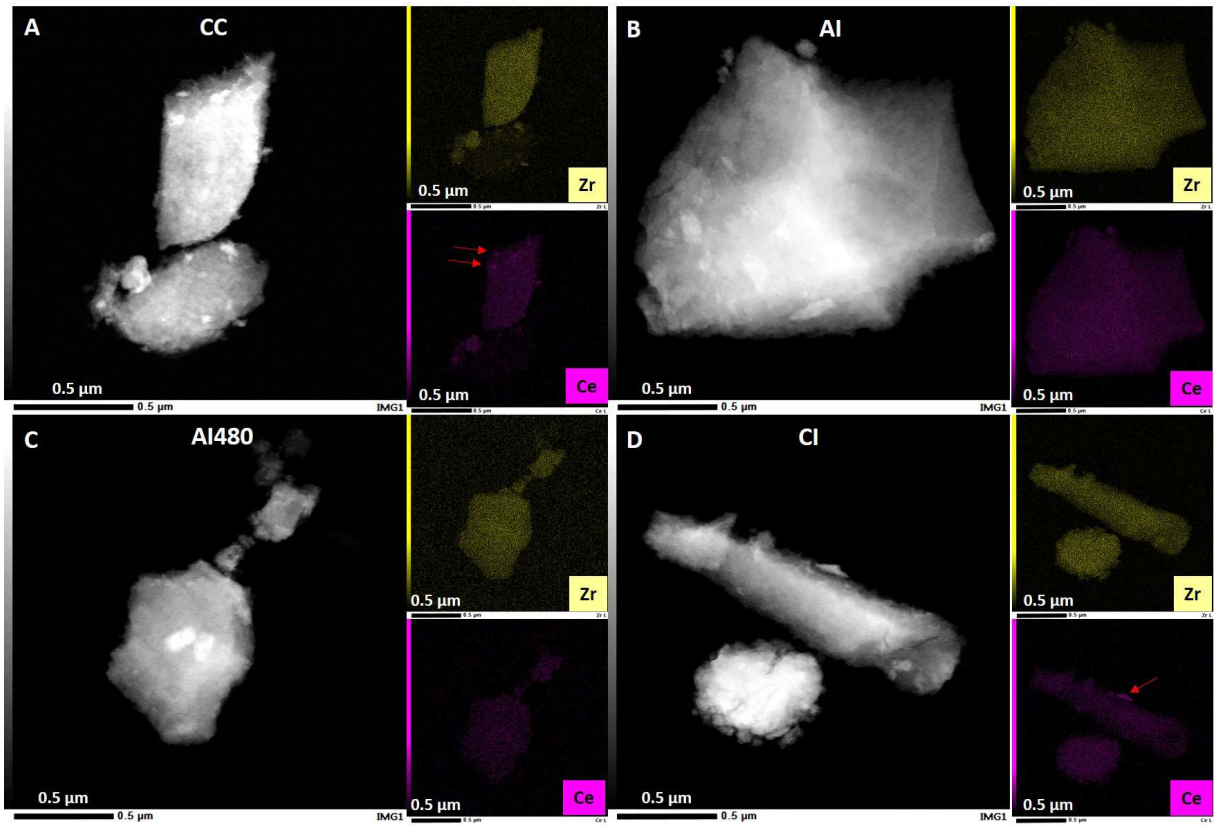

Figure 5

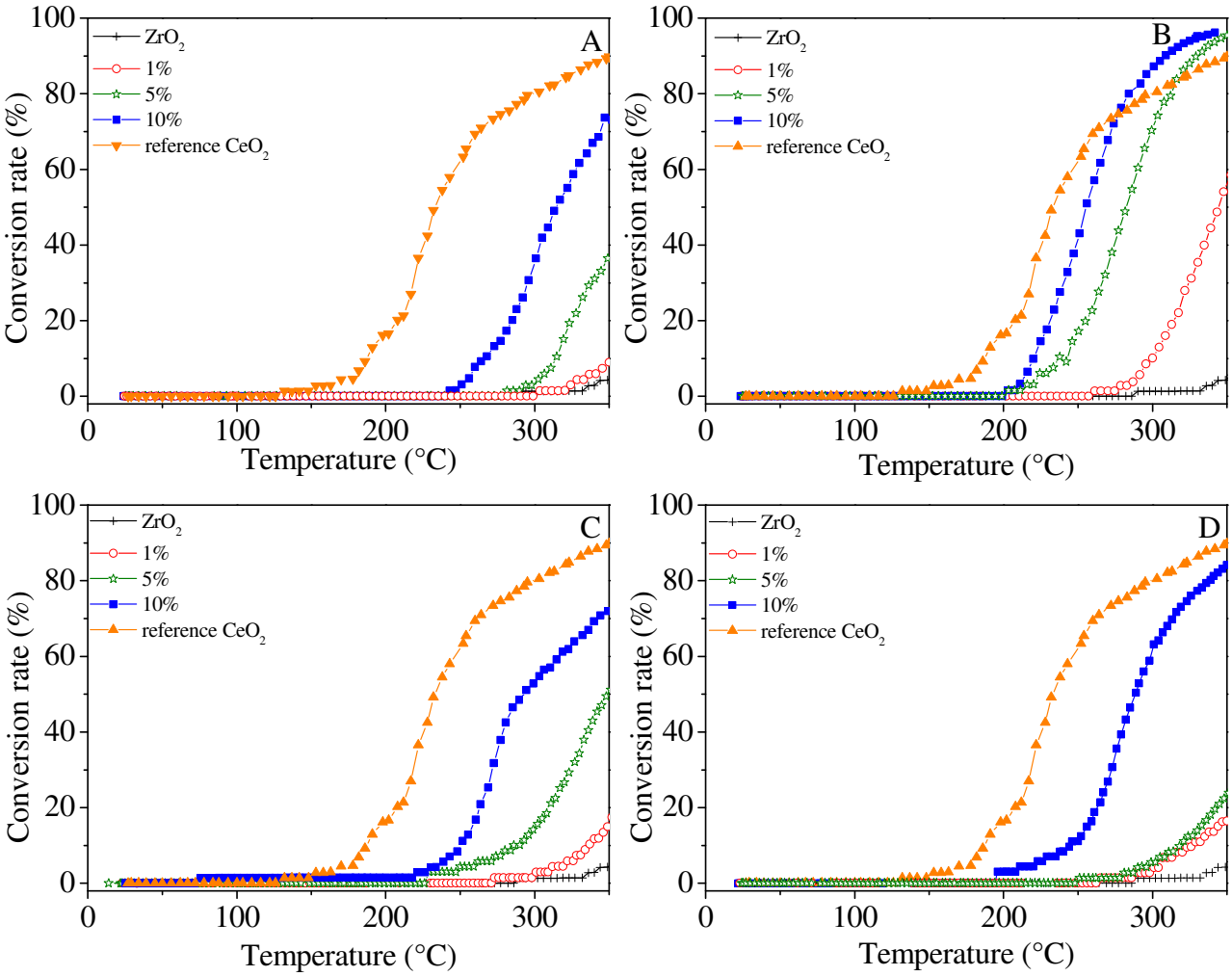
A
B
C
D
ZrO2
1%
5%
10%
reference CeO2
Conversion rate (%)
Temperature (°C)
0
20
40
60
80
100
0
100
200
300

TOC

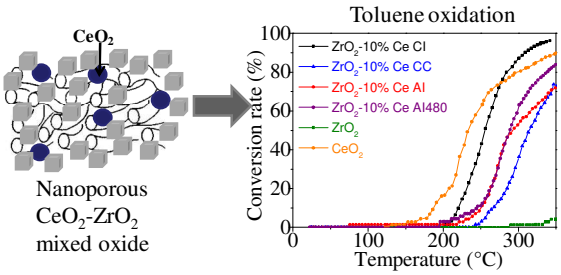
CeO2
Nanoporous
CeO2-ZrO2
mixed oxide
Toluene oxidation
Conversion rate (%)
Temperature (°C)
ZrO2-10% Ce CI
ZrO2-10% Ce CC
ZrO2-10% Ce AI
ZrO2-10% Ce AI480
ZrO2
CeO2